Journal of Power Sources 256 (2014) 258–263

Contents lists available at ScienceDirect

Journal of Power Sources

journal homepage: www.elsevier.com/locate/jpowsour

Exploration of ion migration mechanism and diffusion capability for $Na_3V_2(PO_4)_2F_3$ cathode utilized in rechargeable sodium-ion batteries

Weixin Song [a], Xiaobo Ji [a,*], Zhengping Wu [a], Yingchang Yang [a], Zhou Zhou [a], Fangqian Li [a], Qiyuan Chen [a], Craig E. Banks [b,*]

[a] Key Laboratory of Resources Chemistry of Nonferrous Metals, Ministry of Education, College of Chemistry and Chemical Engineering, Central South University, Changsha 410083, China
[b] Faculty of Science and Engineering, School of Science and the Environment, Division of Chemistry and Environmental Science, Manchester Metropolitan University, Chester Street, Manchester M1 5GD, Lancs, UK

HIGHLIGHTS

- Sodium ion-migration mechanism from/into different Na sites of $Na_3V_2(PO_4)_2F_3$ is investigated.
- Structural reorganization could contribute to three plateaus corresponding to two ions transport.
- The changes in microstructure of the material can influence the ion diffusion capability.
- The diffusion coefficient was firstly calculated with a magnitude of 10^{-12} cm^2 s^{-1} for the $Na_3V_2(PO_4)_2F_3$.

GRAPHICAL ABSTRACT

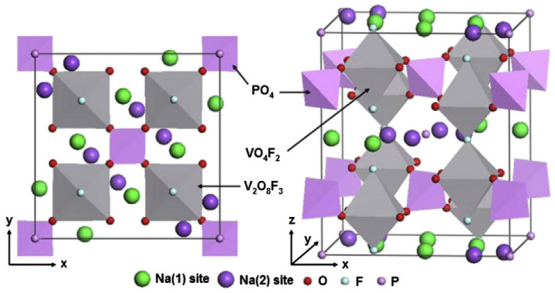

ARTICLE INFO

Article history:
Received 2 December 2013
Received in revised form
27 December 2013
Accepted 6 January 2014
Available online 24 January 2014

Keywords:
NASICON-type $Na_3V_2(PO_4)_2F_3$
Sodium-ion battery
Ion-migration
Diffusion

ABSTRACT

NASICON-type $Na_3V_2(PO_4)_2F_3$ is employed as a promising cathode for sodium-ion batteries in order to explore the ion-migration mechanism and diffusion capability. Two kinds of Na sites, namely Na(1) site and Na(2) site exist in the crystal structure per formula unit to accommodate a total of three sodium ions. The ion at Na(2) site with half occupation extracts first and inserts the last due to its high chemical potential, while the whole extraction/insertion of two ions between 1.6 and 4.6 V *vs.* Na^+/Na can produce three plateaus in charge/discharge processes because of the reorganization of ions. The first discharge capacity of 111.6 mAh g^{-1} with retention of 97.6% after 50 cycles could be obtained by electrochemical testing at 0.091C. Electrochemical activation and/or structural reorganization of the system by cycling could improve the diffusion coefficient of sodium with a comparatively large magnitude of 10^{-12} cm^2 s^{-1}, though many influences on the resistance factors also can be attributed to the cycling process. Such work is of fundamental importance to the progression of sodium-based batteries to be fully realized and be implemented over existing Li-ion based batteries.

1. Introduction

Energy storage systems (ESS) which could efficiently store energy and release it when required have the potential to become key technologies to overcome environmental pollution and gradual depletion of oil resources. Among theses candidates, lithium-ion batteries (LIBs) are the backbone of power sources for a wide

* Corresponding authors.
E-mail addresses: xji@csu.edu.cn (X. Ji), c.banks@mmu.ac.uk (C.E. Banks).

0378-7753/$ – see front matter © 2014 Elsevier B.V. All rights reserved.
http://dx.doi.org/10.1016/j.jpowsour.2014.01.025

range of applications, from electronic devices to increasing numbers of electric vehicles and large-scale energy storage equipments [1–3]. However, the availability of readily-accessible lithium has been questioned due to an ever increasing demand and limited lithium resources [4,5]. Consequently, it is of great importance to find alternative resources to Li, and Na-ion batteries (NIBs) by employing sodium-based electrodes and electrolytes, have been taken into consideration as attractive alternatives to LIBs. Meanwhile, the established understanding of lithium based electrochemical system can be fully taken advantage of to develop the sodium based compounds used in SIBs. For Na-ion batteries, the improved economic efficiency attributed to the rich resources of sodium with corresponding low material cost, as well as no toxicity and ability to utilize electrolytes at low decomposition potentials [6,7] have promoted them as promising ESS.

In the quest for new materials to accommodate this new ESS technology, various kinds of cathode materials have be proposed, such as: Na_2FePO_4F [8], $NaVPO_4F$ [5], NASICON (Na Super-Ionic Conductor)-type $Na_3M_2(PO4)_3$ (M = Ti, Fe, V) [9,10] and $Na_3V_2(PO_4)_2F_3$ [4,11]. Among these, sodium vanadium three-fluorophosphates, $Na_3V_2(PO_4)_2F_3$, one variant of NASICON compounds, recently has been demonstrated to be capable to be used as an excellent candidate for electrodes in hybrid-ion or sodium-ion batteries [4,11]. It has been reported by Meins et al. in 1999 that $Na_3V_2(PO_4)_2F_3$ has a tetragonal crystal structure with the space group of $P4_2/mnm$ by solid state sintering in both high temperature and pressure [12]. Barker et al. reported a graphite/Li^+ electrolyte/$Na_3V_2(PO_4)_2F_3$ hybrid-ion cell with a specific capacity of 126 mAh g^{-1}, and attributed $Na_3V_2(PO_4)_2F_3$ as a potential cathode material in conventional lithium-ion cells which should undergo mixed Li/Na migration. While the presence of appropriate Na^+ ion which extracted from the NASICON structure in initial charging in the electrolyte appeared not to be detrimental to the long-term performance characteristics of the cell [13]. Meanwhile, $Na_3V_2(PO_4)_2F_3$ has been viewed as enabling sodium-based cathodes in a cell configuration with a lithium inserting anode, such as $Li_{4/3}Ti_{5/3}O_4$/Li^+ electrolyte/$Na_3V_2(PO_4)_2F_3$ without the requirement for ion exchange prior to cell fabrication to produce a Li-rich electrode [14]. $Na_3V_2(PO_4)_2F_3$/C composites were successfully prepared by Jiang et al. by sol–gel method with a carbon content of 8.5 wt.%. The reversible capacity of 117 mAh g^{-1} along with good capacity retention was reported and ascribed to the NASICON-type structure with a large ion diffusion coefficient of 7.2×10^{-10} cm^2 s^{-1} in a $Na_3V_2(PO_4)_2F_3$/$LiPF_6$/Li cell [15]. Gover et al. pointed out that all three Na ions might be successfully extracted from the fluorophosphates phase, $Na_3V_2(PO_4)_2F_3$ when the voltage can applied to 5 V (*vs.* Li) although this process was likely accompanied by some concurrent structural degradation [16]. Furthermore, Kang et al. have investigated the electrochemical behaviors of $Na_3V_2(PO_4)_2F_3$ associated with Na ion insertion/extraction by a combined first principles and experimental study [4]. In their conclusions, the phase structure could remain quite stable upon ion extraction and insertion of sodium, of which two sites namely Na(1) site and Na(2) site were utilized to accommodate these sodium ions. However, two Na(1) sites could be fully occupied while the other two Na(2) sites were only half occupied by Na ions because of the large electrostatic repulsions of Na–Na which could not make the Na(2) sites simultaneously occupied. From the structural analysis, the reversible sodiation/desodiation could take place via one-phase reaction with producing negligible variation in lattice parameters (~1%) and cell volume (~2%), thereby, the diffusion of Na ions in the structure would be facilitated and the caused distortion of the crystal lattice would be minimal [4].

Up to now, very few studies have been reported for $Na_3V_2(PO_4)_2F_3$ as use within a sodium-ion battery, especially reporting on the sodium diffused capability since it is crucial in improving the electrochemical performances. Herein, a $Na_3V_2(PO_4)_2F_3$/$NaClO_4$/Na sodium-ion system has been employed for exploration to the sodium ion diffusion capability, as well as the properties for the potential cathode.

2. Experimental section

$Na_3V_2(PO_4)_2F_3$ was prepared by carbothermal reduction (CTR) methodology using a solvation-based precursor. Firstly, stoichiometric amounts of analytical purity Na_2CO_3, $NH_4H_2PO_4$, NaF and V_2O_5 were adequately dissolved into distilled water and dried under 50 °C by forced-air drying. Then, acetylene black powders as reducer and conductive agent (5 wt.%) are mixed in the above-mentioned precursor. Afterward, the mixed precursor was ground to a uniformly particle distribution, then preheated at 350 °C in flow argon for 4 h, and reground before being re-fired at 650 °C in argon atmosphere for 8 h.

The crystallographic structure of the as prepared material was studied by X-ray powder diffraction (XRD) using a Bruker D8 diffractometer with monochromatic Cu Kα radiation ($\lambda = 1.5406$ Å), and the diffraction data was recorded in the 2θ range of 10–60° with a scan rate of 8° min^{-1}. The particle morphology of the composite was investigated by a FEI Quanta 200 scanning electron microscopy (SEM). The thermogravimetric analysis (TG) of the samples was carried on a Diamond TG thermo-analyzer.

The cathode electrode was fabricated with the active material, acetylene black, and binder (Polyvinylidene Fluoride, PVDF) in a weight ratio of 8:1:1 by using NMP as solvent and an aluminum foil as current collector (~4.5 mg cm^{-2}), followed by drying in vacuum at 110 °C for 24 h. The R2016 coin cell was assembled in an argon-filled glove box using alkali foil (lithium or sodium) as the anode with a Celgard 2500 membrane as separator. The electrolyte was 1 M $NaClO_4$ dissolved in polycarbonate (PC). Cyclic voltammetry (CV) and galvanostatic charge/discharge cycling tests were carried out in a setting voltage range by using an electrochemical workstation (CHI660C) and a CT2001A LAND battery tester, respectively. Electrochemical impedance spectroscopy (EIS) was studied using a Modulab (Solartron Analytical) with the amplitude of 5 mV in the frequency range from 1 MHz to 10 mHz. All electrochemical tests were carried out at room temperature.

All calculations on $Na_3V_2(PO_4)_2F_3$ were performed with the spin-polarized Generalized Gradient Approximation (GGA) using the Perdew–Burke–Ernzerhof (PBE) exchange-correlation parameterization to Density Functional Theory (DFT) using CASTEP program. A plane-wave basis with a kinetic energy cutoff of 330 eV was used, and size of standard grid was 1.5. BFGS optimization method was used and the geometry optimization parameters of total energy convergence, max ionic force, max ionic displacement and max stress component tolerance were 0.2×10^{-4} eV $atom^{-1}$, 0.5×10^{-1} eV $Å^{-1}$, 0.2×10^{-2} Å and 0.1 GPa respectively. The electronic convergence thresholds parameters of total energy were 0.2×10^{-5} eV and 0.5638×10^{-6} eV.

3. Results and discussion

Fig. 1 represents the observed experimental XRD patterns of the as-prepared material after refinement, as well as the calculated results from an optimizing DFT refinement of which the referred data are from *The Landolt–Börnstein Database in Springer Materials*. The refined lattice parameters are $a = b = 9.05$ Å, $c = 10.679$ Å, $V = 874.64$ $Å^3$ according to the observed XRD patterns, and $a = b = 9.047$ Å, $c = 10.705$ Å, $V = 876.24$ $Å^3$ based on the DFT calculation, while these structural parameters could be indexed in a $P4_2/mnm$ space group which agree well with preciously reported

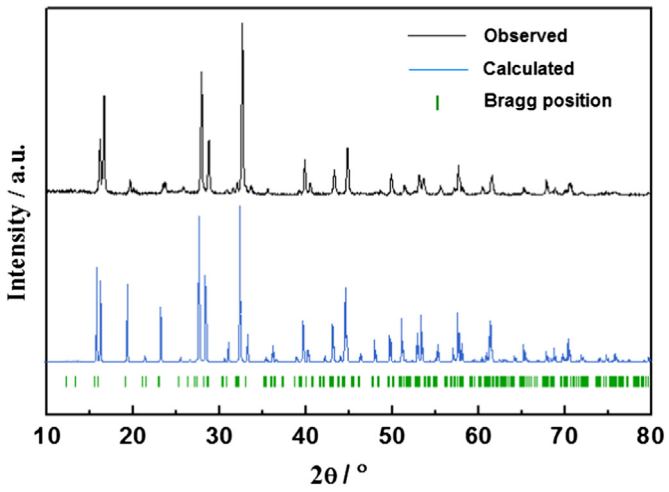

Fig. 1. X-ray diffraction analysis for as-prepared $Na_3V_2(PO_4)_2F_3$.

values [12,16]. Both patterns mostly seem to be in a good agreement with each other though some peak locations and intensities are different, which could be attributed to the optimization in DFT calculations with a crystalline structure.

The crystal structure of $Na_3V_2(PO_4)_2F_3$ projected on the *xy* plane and *xz* plane are displayed in Fig. 2 from which a three-dimensional (3D) NASICON framework can be observed. It is found that this crystal structure is built up from $[V_2O_8F_3]$ bi-octahedral and $[PO_4]$ tetrahedral units. $[V_2O_8F_3]$ bi-octahedra is bridged with two $[VO_4F_2]$ octahedral united by one fluorine atom, whereas the oxygen atoms are all interconnected through the $[PO_4]$ units. Consequently, the arrangement in the NASICON structure has led to the formation of channels along *x* and *y* directions, producing the resultant sodium located tunnel sites. Two triangular prismatic sites surrounded by two F ions and four O ions are denoted as Na(1) sites, while the other two augmented triangular prismatic sites attached to the F apex-square pyramid are denoted as Na(2) sites, where two Na(1) sites are fully occupied and the other two Na(2) sites are half occupied by sodium ions in $Na_3V_2(PO_4)_2F_3$ [4]. Obviously, the diffusion capability of sodium ions should depend on the pathways provided by the formed channels and the accommodated environment of sodium ions.

SEM images of the as-prepared $Na_3V_2(PO_4)_2F_3$ morphology are depicted in Fig. 3. The existence of porosity/pores in these irregularly shaped particles are likely to be helpful for ion diffusion, while the residual carbon in the material previously indicated as an amorphous state could be useful for conductivity between

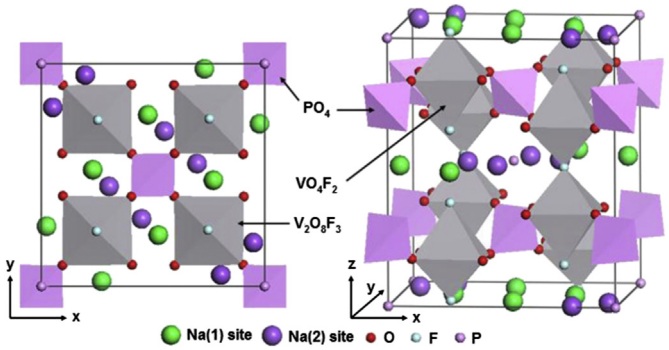

Fig. 2. Representation of the structure of $Na_3V_2(PO_4)_2F_3$.

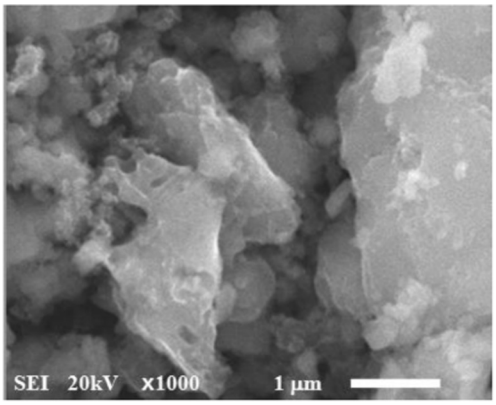

Fig. 3. SEM micrograph of as-prepared $Na_3V_2(PO_4)_2F_3$.

particles. The carbon content was estimated to correspond to 9.2% as obtained by the TG test in an air atmosphere, as shown in Fig. 4.

In all cases the electrochemical characterization of the cathode was carried out in metallic sodium half cells in conjunction with a sodium-based $NaClO_4$ electrolyte. Fig. 5 depicts the initial CV curve of the as-prepared $Na_3V_2(PO_4)_2F_3$ at 0.1 mV s^{-1} in a voltage range of 2.5–4.6 V *vs.* Na^+/Na. There are three couples of redox peaks presented in the cyclic voltammetric scan with oxidation peaks located at 3.44 V, 3.73 V, 4.13 V, and reduction peaks locating at 3.29 V, 3.47 V, 3.96 V, respectively. However, two sodium ions per formula unite have been reported to be able to extract successfully in a upper limited voltage of 4.6 V *vs.* Li^+/Li [16] or 4.5 V *vs.* Na^+/Na [4], while a cathode composition approximating to $NaV_2(PO_4)_2F_3$ would be produced with a condition in which all the vanadium has been oxidized to V^{4+}. Gover et al. have claimed that the differential capacity plot from the Electrochemical Voltage Spectroscopy (EVS) technique depicted a rather complex series of phenomenon occurring during both the charge and discharge processes [16]. Combined with the conclusion from the first principle calculations, Na ions at Na(2) sites are less stable than at Na(1) sites because Na ions at the Na(2) sites are far shifted from the stable position, thereby have a higher chemical potential which indicates that the ions could extract or insert at an earlier stage of charge or later stage of discharge. Thus, the first two redox couple should be responsible for the Na extraction/insertion from/into the Na(2) sites. When half Na ion in one Na(2) site has extracted during

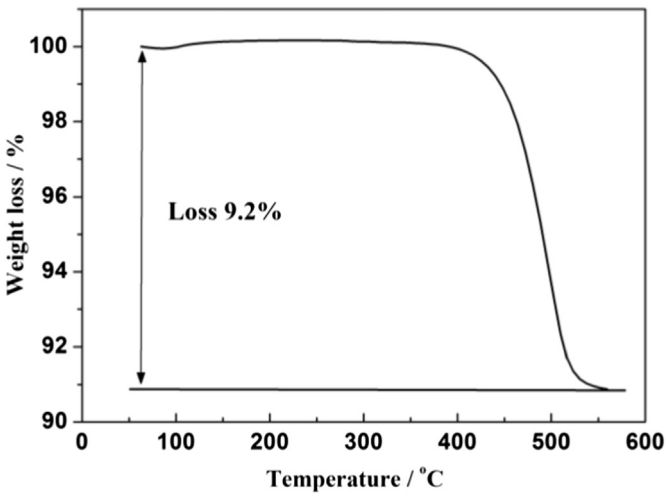

Fig. 4. TG curves of the as-prepared $Na_3V_2(PO_4)_2F_3$.

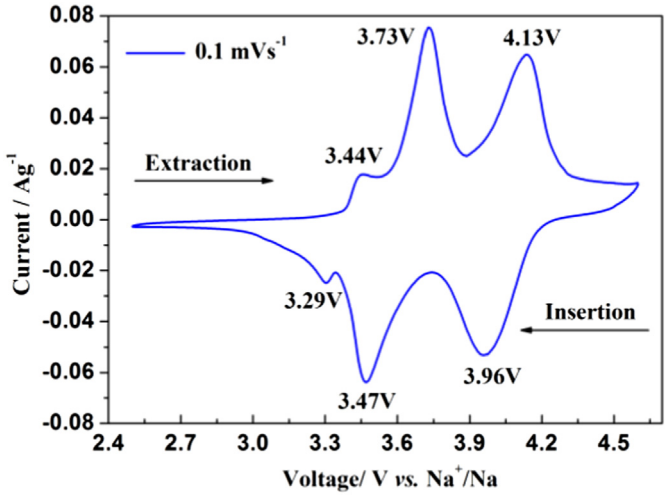

Fig. 5. Initial CV curve of the as-prepared $Na_3V_2(PO_4)_2F_3$ at 0.1 mV s^{-1} in a voltage range of 2.5–4.6 V *vs.* Na^+/Na.

charging, the configuration of $Na_{2.5}V_2(PO_4)_2F_3$ would be expected to be reorganized to a stable state, rendering a different extraction environment for the half Na ion in the other Na(2) site. The left Na ion in Na(2) site becomes stable enough to need more energy to be extracted, consequently another anodic peak would be present at a higher voltage. Similar to the analysis of the variation when the second Na ion extracts, $Na_2V_2(PO_4)_2F_3$ would be reorganized to increase the distance between Na ions in Na(1) sites because the short Na–Na distances (2.92 Å) could make the un-reorganized configuration comparatively unstable. As a result, a higher potential could lead to the extraction of the second Na ion producing a third CV anodic peak, and vice versa for the reduction process.

Fig. 6(a) shows the first charge/discharge profiles of $Na_3V_2(PO_4)_2F_3$/Na cell at a current density of 0.045C and 0.091C (1C denoted as 128 mA g^{-1} corresponding to two sodium ions extraction) in a voltage range of 1.6–4.6 V, respectively. There are two main plateaus with average voltages of about 4.1 V and 3.6 V presenting an average discharge voltage (~3.85 V) which is one of the highest among cathode materials by using the same redox couple V^{3+}/V^{4+} as a consequence of the voltage range from 2.7 V to 3.7 V *vs.* Li^+/Li for vanadium oxides such as V_2O_5, LiV_3O_8 and $Na_3V_2(PO_4)_3$ [4,10,17]. The initial discharge capacities under 0.045C and 0.091C are 114.6 and 111.6 mAh g^{-1}, respectively. The high voltage battery could perform a discharge capacity of 109 mAh g^{-1} (97.6% retention) with a coulombic efficiency of 98% under 0.091C for the extended 50th cycle as shown in Fig 6(b). Phase transformation associated with V^{3+}/V^{4+} would be accompanied to be occurring in the electrochemical process to realize the redox reaction of $Na_xV_2(PO_4)_2F_3$ ($1 \leq x \leq 3$) just as the analyzed electrochemical voltage–composition curve at 0.045C in 1.6–4.6 V during the first cycle shown in Fig. 7. By the function between the net spin moment integrated and the distance from the ion core for $Na_3V_2(PO_4)_2F_3$, Kang et al. concluded that the electrochemical activity of $Na_xV_2(PO_4)_2F_3$ at $1 \leq x \leq 3$ was mainly attributed to V^{3+}/V^{4+} redox reaction. Meanwhile, the strong inductive effects of a fluorine ion as well as a phosphorous ion would shift up the equilibrium potential of the redox couple to make $Na_3V_2(PO_4)_2F_3$ cathode present a high potential.

In the charging process until 3.9 V with $x = 1$, the main plateau at 3.6 V as well as another one at 3.4 V would together contribute to the first Na ion extraction as a result of the reorganization of the cathode system as mentioned above. Thus, the first Na ion could be demonstrated to be extracted in two steps due to an ordered phase

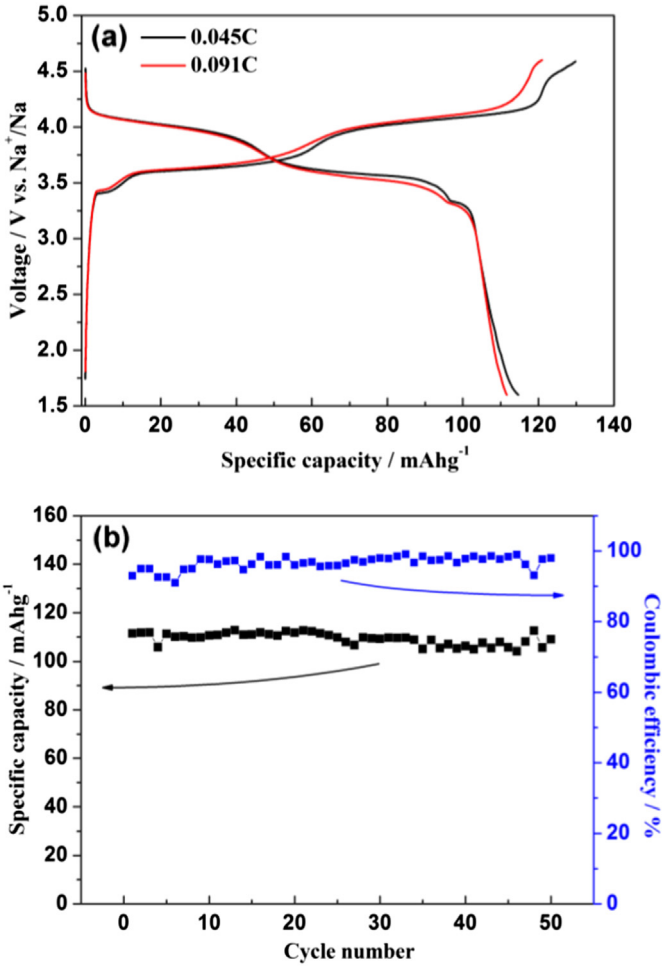

Fig. 6. (a) The first charge/discharge profiles of $Na_3V_2(PO_4)_2F_3$/Na cell at a current density of 0.045C and 0.091C, and (b) the corresponding cyclic performance tested at 0.091C in a voltage range of 1.6–4.6 V.

$Na_{2.5}V_2(PO_4)_2F_3$ which results in a mixed V^{3+}/V^{4+} state. Sequentially, the second Na ion would be removed with a single step (~4.1 V) corresponding to the complete oxidation of V^{3+} to V^{4+}. In the Na^+ insertion process, a solid solution behavior such as the

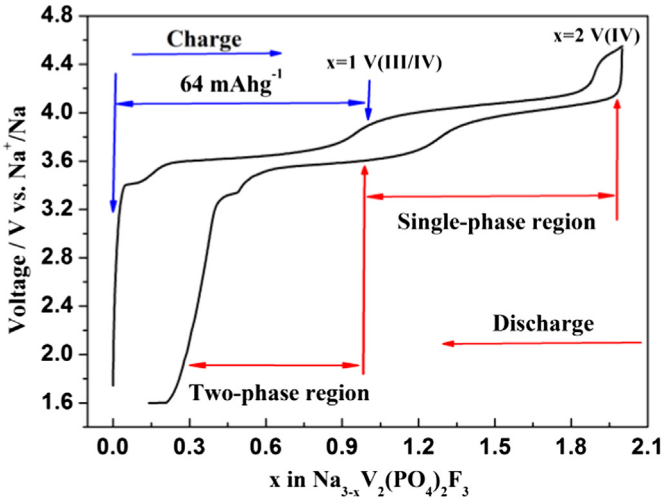

Fig. 7. The electrochemical voltage–composition curve for the $Na_3V_2(PO_4)_2F_3$/Na cell at a current density of 0.045C in a voltage range of 1.6–4.6 V during the first cycle.

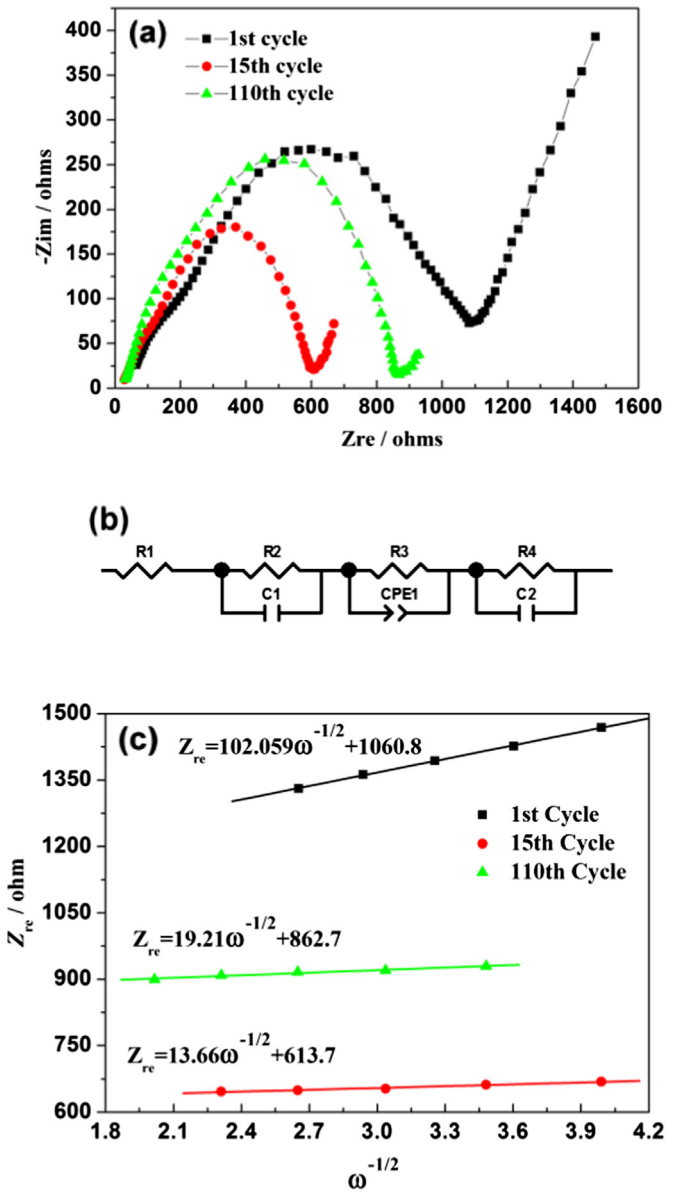

Fig. 8. EIS of the $Na_3V_2(PO_4)_2F_3$/Na cell to derive chemical diffusion coefficient. (a) The Nyquist plots under charged state at 3.7 V for different cycles. (b) The fitting equivalent circuit model for EIS. (c) The plots of the real part of impedance as a function of the inverse square root of angular frequency in the Warburg region.

single-phase region is initially displayed as indicated by the characteristic S-shaped curve [18]. Subsequently, two electrochemical plateaus with little distinction partly due to the relative polarization on the curve exhibits a two-phase behavior, $Na_2V_2(PO_4)_2F_3 \rightarrow Na_{2.5}V_2(PO_4)_2F_3 \rightarrow Na_3V_2(PO_4)_2F_3$ corresponding to the reinsertion of the last Na^+.

EIS, considered as a useful method to identify the chemical diffusion coefficient, was carried out after 1, 15 and 110 cycles at a state of charge of 3.7 V. The Nyquist plots and corresponding fitted equivalent circuit model are given in Fig. 8(a, b). All the impedance parameters with relative errors estimate (%) of the fitting equivalent circuit are listed in Table 1 by using ZSimWin software with each chi-squared function (χ^2) less than 10^{-4}, by which the value of chi-squared function between 10^{-5} and 10^{-4} could provide a reasonably good indication of the quality of the fit [19]. *R*1 represents the internal resistance involving the resistance of the electrolyte and electrode which is denoted as the small intercept at the Z_{re} axis. *R*2 corresponds to the resistance of SEI film as depicted in the high frequency region of the semi-circle, while *C*1 signifies the resultant capacitance from SEI film. *R*3 is the charge transfer resistance in the intermediate-frequency region and *CPE*1 is related to the surface property of the electrode. *R*4 denotes the Warburg resistance originated from the diffusion of Na^+ ions in the electrode bulk as depicted in the low frequency region of the sloping line. *C*2 demonstrate the double layer capacitance caused by ion transfer in the electrode material. After the battery had undergone 1, 15 and 110 cycles, *R*1 seems stable with only little change, while *R*2 decreases firstly and then increases. SEI film formed in the initial cycle is unstable and uneasy for the percolation of the electrolyte, reasonably causing a huge resistance. However, the resistance would go down when the film becomes stable for electrolyte to pass through. But with the increasing cycles the resistance increases again because of the intrinsic character and augmenting thickness of SEI film. A similar changed rule of *R*3 takes place during cycling, and the reason for that could be ascribed to an electrochemically activated process in the first several cycles to render the particles activation. The charge transfer resistance is strongly influenced by cycling as reported [15], mainly due to the enlarging polarization of the electrode during long-time cycling. Warburg impedance *R*4 descends faster in the previous 15 cycles compared with the value of the 110th cycle which could be almost recognized as a stable resistance. This is because the pathways for ion diffusion have become facilitated during cycling which could attribute to the changes in microstructure of the electrode materials.

Thus, the variation and capability of Na ion diffusion of the material is interesting and crucial to the whole electrochemical properties. Ion diffusion coefficient as a vital role to estimate the capability of ion transport, could be evaluated by Equation (1) [20]:

$$D = 0.5R^2T^2/S^2n^4f^4C^2\sigma^2 \quad (1)$$

where *D* is the diffusion constant, *R* the gas constant, *T* the absolute temperature, *S* the effective contact area between electrode and electrolyte ($S = 0.79$ cm^2), *n* the number of electrons in reaction ($n = 2$), *F* the Faraday constant and *C* ($C = 0.0038$ mol cm^{-3}) the concentration of Na ion in the cathode calculated based on the crystallographic cell parameter of $Na_3V_2(PO_4)_2F_3$. While, σ is the Warburg factor which obeys the following relationship [21]:

$$Z_{re} = R1 + R2 + R3 + R4 + \sigma\omega^{-1/2} \quad (2)$$

where ω is the angular frequency and Z_{re} is the real impendence. σ could be obtained by the plots of the real impedance as a function of the inverse square root of angular frequency in the Warburg region as shown in Fig. 8(c). As a result, the chemical diffusion

Table 1
Impedance parameters of the fitting equivalent circuit from the cell undergoing cycles as denoted in the low right corner.

	*R*1 (Ω cm^{-2})	*R*2 (Ω cm^{-2})	*C*1 (F cm^{-2})	*R*3 (Ω cm^{-2})	*CPE*1 (S s$^{1/2}$ cm^{-2})	*R*4 (Ω cm^{-2})	*C*2 (F cm^{-2})
$Results_1$	19.07	673.4	0.02241	964.22	8.8E-5	233	6.76E-6
Error $(\%)_1$	11.53	6.065	4.695	1.637	5.872	5.326	7.301
$Results_{15}$	19.91	194.9	1.75E-5	409.6	9.14E-5	117.9	0.1268
Error $(\%)_{15}$	2.33	4.511	5.156	2.69	5.025	13.62	11.19
$Results_{110}$	19.76	350.5	8.9E-6	439	0.4493	98.96	2.94E-6
Error $(\%)_{110}$	4.615	4.671	5.721	4.746	3.731	7.865	8.723

coefficients (D) are 0.95×10^{-13} cm^2 s^{-1}, 5.29×10^{-12} cm^2 s^{-1}, 2.68×10^{-12} cm^2 s^{-1} for the 1st, 15th and 110th cycle, respectively. By comparison with the values, the electrochemical activation and structural rearrangement [15] the application of cycling should be responsible for the increase of the diffusion coefficient in the first 15 cycles, while the enhanced irreversible factors in the sequential cycles could make the diffusion decrease. However, the chemical diffusion values of $Na_3V_2(PO_4)_2F_3$ SIBs are much lower than that of $Na_3V_2(PO_4)_2F_3$ LIBs ($0.27–7.6 \times 10^{-10}$ cm^2 s^{-1}) which also could be called hybrid-ion batteries [13,14]. It seems to be reasonable since the Li^+ ions have smaller ionic radius and mass than that of Na^+ ions, which would be facile to migrate with faster ion mobility. Additionally the magnitude of the values in this study are still much higher than that in $LiFePO_4$ measured by Prosini et al. (10^{-16}–10^{-14} cm^2 s^{-1}) [22] and Franger et al. (10^{-14}–10^{-13} cm^2 s^{-1}) [23], which should be on account of the NASICON-type structure of $Na_3V_2(PO_4)_2F_3$ allowing Na^+ ions transport in a much opening 3D framework and resulting in a high ion diffusion capability.

4. Conclusions

NASICON-type $Na_3V_2(PO_4)_2F_3$ was prepared by a carbothermal reduction methodology and employed as cathode in a sodium-ion battery to investigate the ion migrated mechanism and diffusion capability. There are two kinds of Na sites namely Na(1) site and Na(2) site to accommodate total three sodium ions per formula unit. The sodium ion at Na(2) sites with half occupation could be extracted earlier due to the high chemical potential, and the whole extraction/insertion of two sodium ions in a voltage range from 1.6 to 4.6 V *vs.* Na^+/Na would produce three plateaus in charge/discharge processes due to the reorganization of the cathode configuration when the ions migrate from/into the Na site. An initial capacity of 111.6 mAh g^{-1} with retention of 97.6% after 50 cycles could be obtained by galvanostatic charge/discharge at a current density of 0.091C. The sodium ion diffusion could be improved after the electrochemical activation and/or structural reorganization during cycling to reach a comparatively large value with a magnitude of 10^{-12} cm^2 s^{-1} for the sodium-ion battery.

Acknowledgments

Financial supports from the NNSF of China (No. 51134007, 21003161, 21250110060), Program for the New Century Excellent Talents in University (No. NCET-11-0513), Funds for Distinguished Young Scientists of Hunan Province, China (No. 13JJ1004), Fundamental Research Funds for Central South University (No. 2013zzts159, No. 2012zzts059), Innovation and Entrepreneurship Training Program of China for University Students and the Open-End Fund for the Valuable and Precision Instruments of Central South University (CSUZC2013004) are greatly appreciated.

References

[1] M. Armand, J.M. Tarascon, Nature 451 (2008) 652–657.
[2] Z. Jian, W. Han, X. Lu, H. Yang, Y.-S. Hu, J. Zhou, Z. Zhou, J. Li, W. Chen, D. Chen, L. Chen, Adv. Energy Mater. 3 (2013) 156–160.
[3] C.-X. Zu, H. Li, Energy Environ. Sci. 4 (2011) 2614–2624.
[4] R.A. Shakoor, D.-H. Seo, H. Kim, Y.-U. Park, J. Kim, S.-W. Kim, H. Gwon, S. Lee, K. Kang, J. Mater. Chem. 22 (2012) 20535–20541.
[5] B.L. Ellis, W.R.M. Makahnouk, W.N. Rowan-Weetaluktuk, D.H. Ryan, L.F. Nazar, Chem. Mater. 22 (2010) 1059–1070.
[6] S.-W. Kim, D.-H. Seo, X. Ma, G. Ceder, K. Kang, Adv. Energy Mater. 2 (2012) 710–721.
[7] H. Zhuo, X. Wang, A. Tang, Z. Liu, S. Gamboa, P.J. Sebastian, J. Power Sources 160 (2006) 698–703.
[8] B.L. Ellis, W.R.M. Makahnouk, Y. Makimura, K. Toghill, L.F. Nazar, Nat. Mater. 6 (2007) 749–753.
[9] H. Kabbour, D. Coillot, M. Colmont, C. Masquelier, O. Mentre, J. Am. Chem. Soc. 133 (2011) 11900–11903.
[10] W. Song, X. Ji, C. Pan, Y. Zhu, Q. Chen, C.E. Banks, Phys. Chem. Chem. Phys. 15 (2013) 14357–14363.
[11] W. Song, S. Liu, Solid State Sci. 15 (2013) 1–6.
[12] J.M. Le Meins, M.P. Crosnier-Lopez, A. Hemon-Ribaud, G. Courbion, J. Solid State Chem. 148 (1999) 260–277.
[13] J. Barker, R.K.B. Gover, P. Burns, A.J. Bryan, Electrochem. Solid-State Lett. 9 (2006) A190–A192.
[14] J. Barker, R.K.B. Gover, P. Burns, A.J. Bryan, J. Electrochem. Soc. 154 (2007) A882–A887.
[15] T. Jiang, G. Chen, A. Li, C.Z. Wang, Y.J. Wei, J. Alloys Compd. 478 (2009) 604–607.
[16] R.K.B. Gover, A. Bryan, P. Burns, J. Barker, Solid State Ionics 177 (2006) 1495–1500.
[17] J.M. Tarascon, M. Armand, Nature 414 (2001) 359–367.
[18] X.H. Rui, N. Ding, J. Liu, C. Li, C.H. Chen, Electrochim. Acta 55 (2010) 2384–2390.
[19] M. Umeda, K. Dokko, Y. Fujita, M. Mohamedi, I. Uchida, J.R. Selman, Electrochim. Acta 47 (2001) 885–890.
[20] X. Liao, Z. Ma, Q. Gong, Y. He, L. Pei, L. Zeng, Electrochem. Commun. 10 (2008) 691–694.
[21] H. Liu, C. Li, Q. Cao, Y. Wu, R. Holze, J. Solid State Electrochem. 12 (2008) 1017–1020.
[22] P.P. Prosini, M. Lisi, D. Zane, M. Pasquali, Solid State Ionics 148 (2002) 45–51.
[23] S. Franger, F. Le Cras, C. Bourbon, H. Rouault, Electrochem. Solid-State Lett. 5 (2002) A231–A233.